Copyright © 2010 Tech Science Press CMES, vol.56, no.1, pp.1-16, 2010

Size Effects and Mesh Independence in Dynamic Fracture Analysis of Brittle Materials

Letícia Fleck Fadel Miguel[1], **Ignacio Iturrioz**[2] **and Jorge Daniel Riera**[3]

Abstract: Numerical predictions of the failure load of large structures, accounting for size effects, require the adoption of appropriate constitutive relations. These relations depend on the size of the elements and on the correlation lengths of the random fields that describe material properties. The authors proposed earlier expressions for the tensile stress-strain relation of concrete, whose parameters are related to standard properties of the material, such as Young's modulus or specific fracture energy and to size. Simulations conducted for a typical concrete showed that as size increases, the effective stress-strain diagram becomes increasingly linear, with a sudden rupture, while at the same time the coefficients of variation (CV) of the relevant parameters decrease to negligible values, situation that renders Linear Elastic Fracture Mechanics (LEFM) applicable. However, it was later observed that a hitherto unknown problem arises in the analysis of non-homogeneous materials, leading to lack of mesh objectivity: the need to know a priori the degree of fracturing. This should affect not only the truss-like Discrete Element Method (DEM) employed herein, but also finite element analysis, requiring a careful evaluation of the energy dissipated by fracture or other mechanisms in the course of the loading process. In the paper a tentative criterion is proposed to account for the effect in non-linear dynamic fracture analysis.

Keywords: Scale Effect, Mesh Objectivity, Fracture, Brittle Materials, Discrete Element Method.

1 Introduction

The authors determined numerically the response of geometrically similar reinforced concrete beams built in four different sizes, tested to rupture by Leonhart and Walter (1961) and later reproduced by Ramallo *et al.* (1995), to quantify size

[1] Department of Mechanical Engineering, UFRGS, Porto Alegre, Brazil. letffm@ufrgs.br
[2] Department of Mechanical Eng., UFRGS, Porto Alegre, Brazil. ignacio@mecanica.ufrgs.br
[3] Department of Civil Engineering, UFRGS, Porto Alegre, Brazil. jorge.riera@ufrgs.br

effects in reinforced concrete beams. For such purpose the so-called truss-like Discrete Element Method (DEM) was employed, modeling inhomogeneneities in concrete and steel by assuming that their stiffness and specific fracture energies are random fields in 3D-space. The constitutive criteria was based on Hillerborg's model (1971) and presented improvements in the consideration of the spatial correlation of the random fields. The discrete numerical model was also used to reproduce experimental results due to van Vliet and van Mier (2000) concerning the influence of sample size on the tensile strength of concrete and rock samples as well as the theoretical strength of large rock dowels subjected to shear (Miguel *et al.*, 2008). In all cases, in order to represent the stress-strain relation for concrete in tension, a triangular diagram was employed, which proves adequate when the size of the elements is sufficiently small and the inhomogeneous properties of the material are properly accounted for. These conditions require large DEM or FEM models, which cannot be usually employed in engineering practice due to cost-effectiveness considerations. In a previous paper Riera and Iturrioz (2007) contend that predictions of the failure load of concrete structures, accounting for size effects, can be made using larger elements and therefore reduced computational costs, if the appropriate stress-strain relations are adopted. These relations depend both on the size of the element and on the correlation lengths of the random fields that describe the relevant material properties.

In response determinations of structures with initial cracks or high stress gradients, which result in fracture localization, well established procedures lead to results that are mesh independent. However, in elements subjected to approximately uniform stress fields, a hitherto scarcely noticed problem arises in the analysis of non-homogeneous materials: the need to know a priori the degree of fracturing of the element (Iturrioz *et al.*, 2009). This should also affect finite element analysis in cases in which there is no clear fracture localization, requiring a careful evaluation of the energy dissipated by fracture or other mechanisms in the course of the loading process (van Mier, 2003). In the paper, a tentative criterion is proposed to account for this effect in non-linear dynamic fracture analysis of large structural systems.

2 The discrete element method in fracture problems

The truss-like Discrete Element Method employed in this paper is based on the representation of a solid by means of an arrangement of one dimensional elements able to carry only axial loads. The equivalence between an orthotropic elastic continuum and the cubic arrangement of uni-axial elements consisting of a cubic cell with eight nodes at its corners plus a central node was shown by Nayfeh and Hefzy (1978). The discrete elements representation of the orthotropic continuum was

adopted by the authors to solve structural dynamics problems by means of explicit direct numerical integration of the equations of motion, assuming the mass lumped at the nodes. Each node has three degrees of freedom, corresponding to the nodal displacements in the three orthogonal coordinate directions.

The equivalence between the orthotropic elastic solid with orthotropic axes oriented in the direction parallel to the longitudinal elements of the discrete elements model was extensively verified in previous contributions of the authors. The equations that relate the properties of the elements with the elastic constants of an isotropic medium are:

$$\delta = \frac{9\nu}{4-8\nu}, \quad EA_n = EL_0^2 \frac{(9+8\delta)}{2(9+12\delta)}, \quad EA_d = \frac{2\sqrt{3}}{3} A_n \tag{1}$$

in which E and ν denote Young's modulus and Poisson's ratio, respectively, while A_n and A_d represent the areas of normal and diagonal elements.

The resulting equations of motion may be written in the well-known form:

$$\mathbf{M}\ddot{\vec{x}} + \mathbf{C}\dot{\vec{x}} + \vec{F}_r(t) - \vec{P}(t) = \vec{0} \tag{2}$$

in which $\vec{x}$ represents the vector of generalized nodal displacements, $\mathbf{M}$ the diagonal mass matrix, $\mathbf{C}$ the damping matrix, also assumed diagonal, $\vec{F}_r(t)$ the vector of internal forces acting on the nodal masses and $\vec{P}(t)$ the vector of external forces. Obviously, if $\mathbf{M}$ and $\mathbf{C}$ are diagonal, Equations (2) are not coupled. Then the explicit central finite differences scheme may be used to integrate Equation (2) in the time domain. Since the nodal coordinates are updated at every time step, large displacements can be accounted for in a natural and efficient manner. In this paper, the relation between tensile stress and strain in the material was assumed triangular (Figure 1). The limit strain ε_r is determined to satisfy the condition that, upon rupture of the element, once the strain reaches the value ε_r, a fracture energy U_{elem} is dissipated, according to Equation (3):

$$U_{elem} = \frac{A_f G_f}{L_0} \tag{3}$$

in which A_f is the fractured area of the discrete element, L_0 is its length and G_f is the specific fracture energy that characterized the material toughness. Note that the fracture energy, *i.e.*, the energy dissipated by the total rupture of one element, depends on the numerator of Equation (3), which is the product of the fractured area within the element times the specific fracture energy of the material.

In previous papers (Riera and Iturrioz, 1998; Miguel *et al.*, 2008), it was assumed that A_f equals the area L_0^2 of a cubic brick of the truss-like model. On that basis,

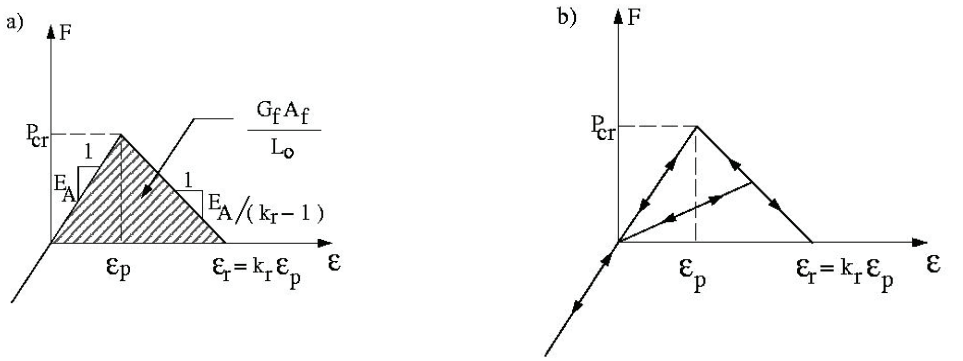

Figure 1: Triangular constitutive law for brittle materials.

the fracture area of an individual element is given by:

$$A_f = c_a L_0^2 \tag{4}$$

in which the coefficient c_a was obtained as follows: if a single crack splits the cube shown in Figure 2 in two parts, the contribution of individual members to the fracture energy $G_f\ L_0^2$ is given by the right-hand side of Equation (5):

$$G_f L_0^2 = G_f \left[4 \times 0.25 \times c_a L_0^2 + c_a L_0^2 + 4 c_a \left(1.15 L_0\right)^2\right] \tag{5}$$

Which leads to $c_a = 0.1385$.

The coefficients indicated above are applicable as long as there is a strong localization effect, leading to a rupture configuration characterized by a single crack traversing each cubic cell of sides with length L_0. One such example is fracture of a rock dowel (Miguel *et al.*, 2008), which occurs in most cases in the form of a crack that, starting near the intersection of the dowel wall and the base, propagates through the dowel.

Another important feature of the approach is the assumption that G_f is not constant throughout the structure. In this paper, a Weibull distribution with coefficient of variation (CV) of 100% was adopted. This value resulted from a limited number of simulations with CV in the range (20, 120), but certainly deserves additional research for each specific material. It should be underlined again that fracture localization weakens as the non-homogeneous nature of the material becomes more pronounced, *i.e.*, as the coefficients of variation of the fields that describe the material properties increase.

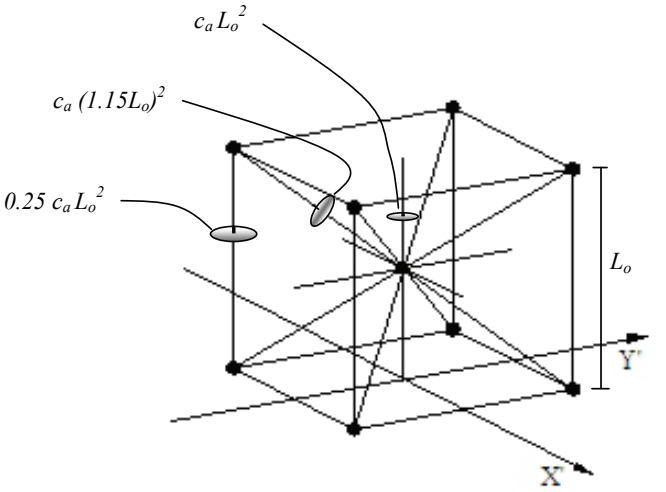

Figure 2: Detail of the cubic array showing the areas of individual members.

Applications of the DEM in studies involving non-homogeneous materials subjected to fracture in which the single crack assumption through each element is valid, may be found in Iturrioz (1995), Riera and Iturrioz (1998), Dalguer *et al.* (2001), Rios and Riera (2004) and Miguel *et al.* (2008). Additionally, Dalguer *et al.* (2003), Riera *et al.* (2005), Miguel (2005), Miguel *et al.* (2006) and Miguel and Riera (2007), contributed to demonstrate the reliability of the approach by comparing DEM predictions with experimental results or other numerical techniques. It is also pertinent to stress that the problem is not a difficulty of the DEM approach, but a basic issue of numerical predictions in Fracture Mechanics (van Mier, 2003). Interesting efforts to predict fracture and fragmentation in solids using finite elements adopting the cohesive interface approach were reported by Needleman (1997) and more recently by Maiti and Geubelle (2004).

Several studies that employ the Meshless Method (MM) to simulate fracture propagation may be cited. Li *et al.* (2008) predict the onset of macroscopic cracking in structures undergoing gross plastic deformations under static loading. Shen (2009) employs the technique to simulate glass fragmentation. Sageresan and Drathi (2008) apply a version of the MM to simulate fracture propagation in concrete, predicting complete load-deformation curves for deformation-controlled tests. Wang and Wang (2008) simulate dynamic crack propagation with branching, while Selvadurai (2009) applied a different version of DEM to analyze impact of ice against a rigid target structure.

3 Size effect in fracture analysis of non-homogeneous cubic samples

3.1 Uniform displacement

Concrete cubic samples fixed at the lower face and subjected to a monotonically increasing uniformly distributed normal displacement on the upper face were analyzed first. The response of each sample up to failure was determined through numerical simulation. The size of the samples ranges from 0.12m to 0.96m. Sample dimensions and the DEM mesh employed in the analysis are indicated in Table 1. The material properties of the material (concrete) are given in Table 2. In the ensuing simulations, only the specific fracture energy was assumed to vary as a 3D random field, while E, ρ and ν were considered constants.

Table 1: Basic dimensions of the concrete samples.

Sample size (m)	**DEM mesh**	L_0 **(m)**
0.12	6×6×6	0.02
0.24	12×12×12	0.02
0.48	24×24×24	0.02
0.72	36×36×36	0.02
0.96	48×48×48	0.02

Table 2: Concrete properties.

Property	**Value**
E (Young's modulus)	3.5E10N/m^2
ρ (mass density)	2400kg/m^3
ν (Poisson's ratio)	0.25
E(G_f) (expected value of specific fracture energy)	100N/m
ε_p (critical strain)	6.3E-5
CV(G_f) (coefficient of variation of G_f)	100%

Nodal points on the upper face of the specimens were subjected to a controlled uniform displacement that increases smoothly in time, inducing a nominally uniform tension in the specimen. Six simulations were performed for each size. The resulting stress-strain curves for all simulations of the 0.12m cube are shown in Figure 3(a) and in Figure 3(b) for all simulations of the 0.96m cube. Note that the fracture energy of the material is regarded as a random field with the properties indicated in Table 2 and Weibull (Minimum Type III) probability distribution function, so each simulated test leads to a different stress-strain curve. As expected, the variability

of the predicted response decreases when the cube size grows. The mean curve for all simulations is also shown in Figure 3, while the mean curves for all sizes are shown in Figure 4.

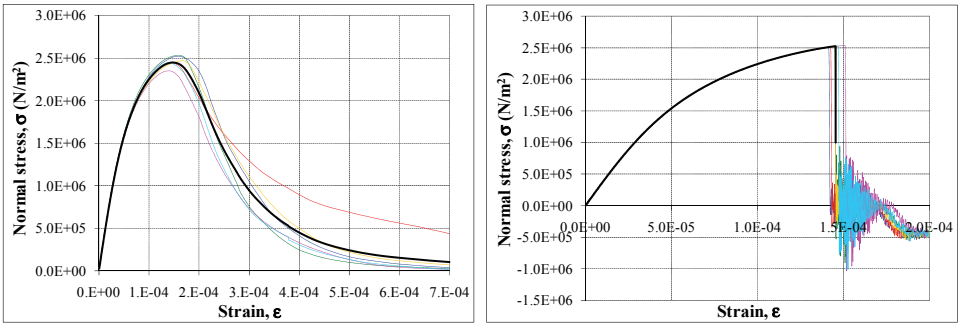

(a) (b)

Figure 3: Normal stress on the lower face *vs.* mean strain for all simulations and resulting mean curve (thick black line), (a) 0.12m cube and (b) 0.96m cube.

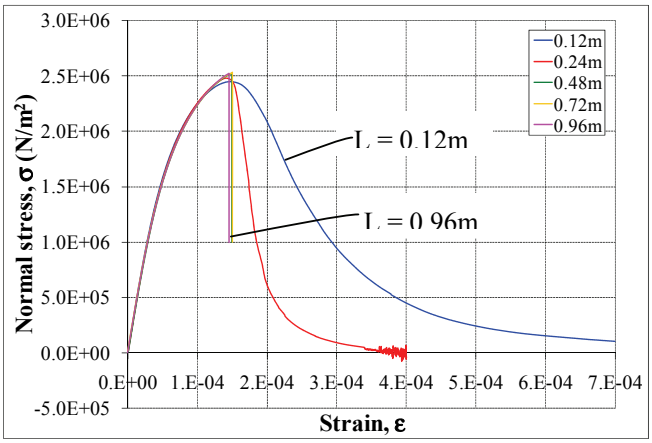

Figure 4: Normal stress on the lower face *vs.* mean strain for the mean curve of all tested sizes (uniformly distributed upper boundary displacements).

Typical crack patterns are shown in Figure 5. Undamaged, damaged and totally broken elements are represented in cyan, orange and red, respectively. The graphs show both a typical fracture pattern, as well as the damage distribution in the cube.

Table 3 presents the average tensile strength and the corresponding strain of the cubes, which are not sensitive to size within the simulation range.

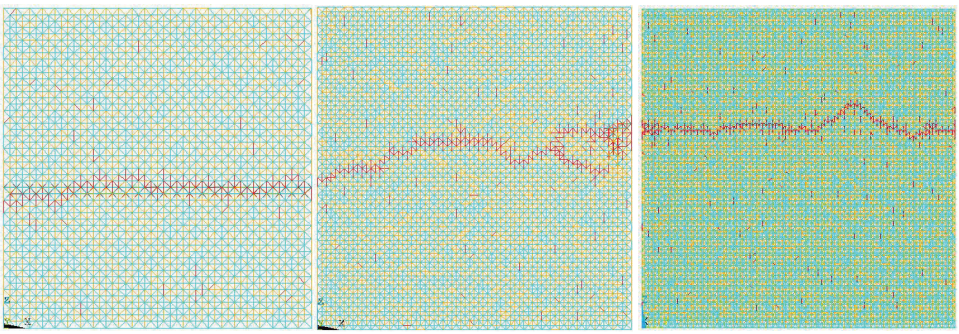

L = 0.48m L = 0.72m L = 0.96m

Figure 5: Rupture configuration of concrete cubes subjected to uniformly distributed prescribed displacements on upper surface. Note that only central slices of the cubes are shown.

Table 3: Mean peak tensile stress and corresponding strain for uniform imposed displacements.

Sample size (m)	**Stress σ_r (MPa)**	**Strain ε_r**
0.12	2.45	1.47E-4
0.24	2.48	1.41E-4
0.48	2.52	1.50E-4
0.72	2.53	1.50E-4
0.96	2.52	1.46E-4

3.2 Triangular displacement

Next, the concrete simulated samples, fixed at the lower face, were subjected to triangularly distributed displacements with constant strain rate on their upper face and analyzed up to failure through numerical simulation. Again, the size of the cubes ranges from 0.12m to 0.96m and cube dimensions and DEM mesh employed in the analysis are indicated in Table 1. The material properties were given in Table 2.

Six simulations were performed for each size. The resulting stress-strain curves for all simulations of the 0.12m cube are shown in Figure 6(a) and for the 0.96m cube

in Figure 6(b), which also presents the mean curve. Direct observation shows that the variability of the predicted response also diminishes when the cube size grows. Figure 7 shows the mean curves for all simulated sample sizes.

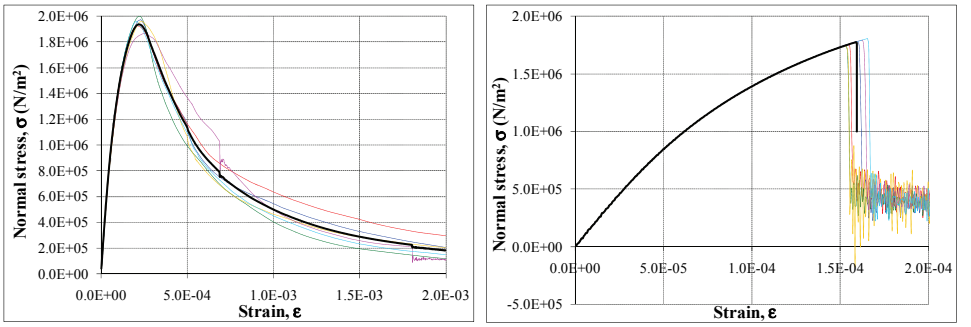

(a) (b)

Figure 6: Normal stress on the lower face *vs.* mean strain for all simulations and resulting mean curve (thick black line), (a) 0.12m cube and (b) 0.96m cube.

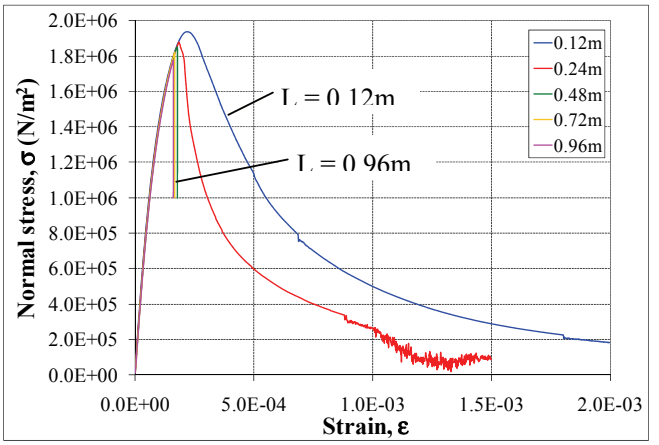

Figure 7: Normal stress on the lower face *vs.* mean strain for the mean curve of all tested sizes (triangular distribution of upper boundary displacements).

Typical crack patterns are shown in Figure 8. Undamaged, damaged and totally broken elements are represented in cyan, orange and red, respectively. The graphs show both a typical fracture pattern, as well as the damage distribution in the cube.

Table 4 presents the average tensile strength and ultimate strain of the cubes, which tend to decrease as the size of the cube increases.

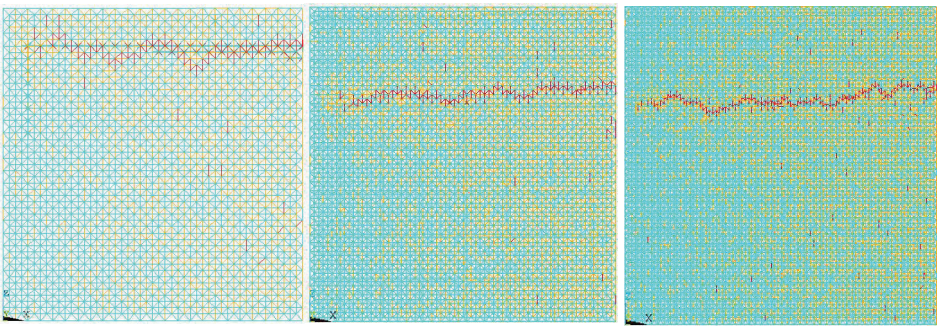

L = 0.48m L = 0.72m L = 0.96m

Figure 8: Rupture configuration of concrete cubes subjected to triangularly distributed prescribed displacements on upper surface. Note that only central slices of the cubes are shown.

Table 4: Mean peak tensile stress and corresponding strain for triangular imposed displacements.

Sample size (m)	**Stress σ_r (MPa)**	**Strain ε_r**
0.12	1.94	2.20E-4
0.24	1.88	1.84E-4
0.48	1.84	1.78E-4
0.72	1.81	1.68E-4
0.96	1.77	1.60E-4

In Figures 5 and 8 it may be seen that damage localization is more pronounced in presence of a stress gradient (triangularly distributed imposed displacements). Both damage, indicated by the orange-tainted regions, as well as crack surfaces, are more widely distributed in case of uniform imposed displacements (Figure 5). Although no experimental results for this size range are known to the authors, the effects unquestionably exist. Therefore, both features of the non-linear problem should be taken into consideration if larger DEM or FEM elements must be resorted to in order to reduce computational costs.

4 Influence of damping in the numerical simulations

The evolution of the fracture process in concrete samples subjected to static tensile loading is determined by explicit numerical integration of the non-linear equations of motion of the system assuming, for such purpose, that in addition to the energy dissipated by fracture, there is also energy dissipated by mass-proportional internal viscous-type damping within the material. It was verified that the response computed with realistic values of the material damping coefficient, estimated so the free vibrations in the fundamental mode of a cubic sample, with no fracture occurring, would be characterized by critical damping ratios in the range between 1 and 2%, differs from the response computed with above critical damping ratios only after the peak load is reached.

Figure 9(a) shows normal stress on the lower face of the samples versus mean strain curves determined by numerical simulation for 0.96m samples, for uniformly distributed imposed displacements, assuming a low, realistic damping coefficient and a very high damping coefficient. Figure 9(b) present similar results for triangularly distributed imposed displacements. It may be seen that the maximum stress and corresponding strain are not affected by the viscous damping coefficient, in spite of the large difference in damping between the samples.

It was thus concluded that internal viscous damping was not an important factor in the assessment of size effects in samples subjected to tensile loading.

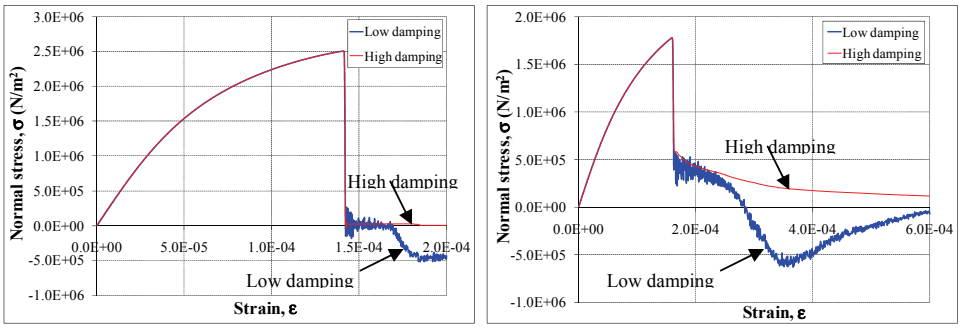

(a) (b)

Figure 9: Comparison between responses computed assuming low and high damping coefficients, for uniformly distributed imposed displacements (Fig.9a) and for triangularly distributed imposed displacements (Fig.9b).

5 Size dependence of fracture energy

Table 5 presents data on the variation of the fracture energy needed to split the specimen in two parts as its size increases. The second column indicates the theoretical minimum energy U_{min}, while the third column shows the energy determined by simulation for nominal uniform stress (or strain) distributions. It was also observed that for triangularly distributed boundary displacements, the fracture energy approaches the theoretical minimum, indicating a strong localization effect.

Figure 10(a) shows the normalized fracture energy versus strain during the fracture process for nominal uniform stress, while Figure 10(b) presents similar information for triangularly distributed imposed displacements. It may be clearly seen that as size increases, the failure strain decreases, *i.e.*, larger specimens of the same material are more fragile. Van Mier (2003) also emphasizes the influence of stress gradients on size effects, which can be explained by the more pronounced damage localization in the presence of stress gradients. Moreover, in a nominally uniform initial stress field, the ratio between the work needed to split the specimen and the theoretical minimum energy (corresponding to an ideal full damage localization) increases with size.

Table 5: Fracture energy needed to split the specimen in two parts in a nominally uniform strain field.

Size (m)	U_{min} **(Nm)**	**E**[U_{num}] **(Nm)**	**E** [U_{num}/U_{min}]	**CV**[U_{num}/U_{min}] **(%)**
0.12	1.44	1.68	1.17	19.0
0.24	5.76	6.85	1.19	17.3
0.48	23.04	34.33	1.49	7.0
0.72	51.84	85.43	1.65	7.9
0.96	92.16	173.72	1.88	15.8

Simulated samples attain the final value of the fracture energy for very large strains, while Figures 10(a) and (b) show only the initial part of the corresponding curves. For the uniform strain field, the final values of the normalized energies are indicated in Table 5. The results in Table 5 and in Figure 10(a) imply that if larger DEM elements are employed in fracture studies, in addition to the stress-strain diagram associated to the element size, the correct c_a coefficient must be used, which is obtained by multiplying the value 0.1385, calculated on the assumption of a single crack across the element, by the coefficient in the fourth column of Table 5. This correction would allow considering the occurrence of additional damage, beyond the failure surface, as shown by Figure 5.

Carpinteri and Chiaia (2002) consider this effect by introducing the notion of frac-

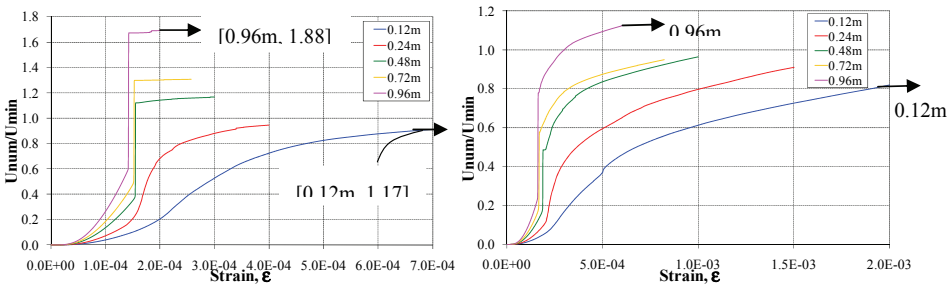

(a) (b)

Figure 10: Expected value of the normalized fracture energy *vs.* strain during the fracture process, for uniform imposed displacements (Fig.10a) and for triangular imposed displacements (Fig.10b).

tal dimension, linked to fractured area as defined in this study, when the fractal dimension is higher than 2. Figure 11 shows a comparison between the relation for a dimension (d = 2.3) as proposed by Carpinteri and Chiaia (2002) and DEM simulations reported herein, for uniform imposed displacements. A fit of the equation proposed by Carpinteri and Chiaia (2002) to simulated values obtained with DEM models led to a mean fractal dimension d = 2.29, which is a surprisingly close correlation, since present results should be dependent on the assumed material properties. The corresponding curve is also shown in Figure 11. Note that the 0.12m cube was adopted for this comparison as the smallest representative sample of the material. It is also clear that both curves in Figure 11 constitute a limit case, applicable in the absence of strong stress gradients. In fact, as pointed out by van Mier (2003), the strain softening branch of the nominal stress-strain relation is not really a material property, since it is affected by the applied loading.

6 Conclusions

It was confirmed in this examination of the tensile fracture behavior of concrete cubic samples that predictions of fracture of non-homogeneous materials using DEM models are feasible and yield results that are consistent with the experimental evidence so far available. The use of large elements, in which extensive cracking within the elements of the model may be expected, requires the consideration of the increase with size of the fractured area, in addition to the effective stress-strain curve for the element. This is a basic requirement in order to achieve mesh objectivity. Note that the degree of damage localization must be known *a priori*, which is a still unresolved difficulty of the non-linear fracture analysis of non-homogeneous

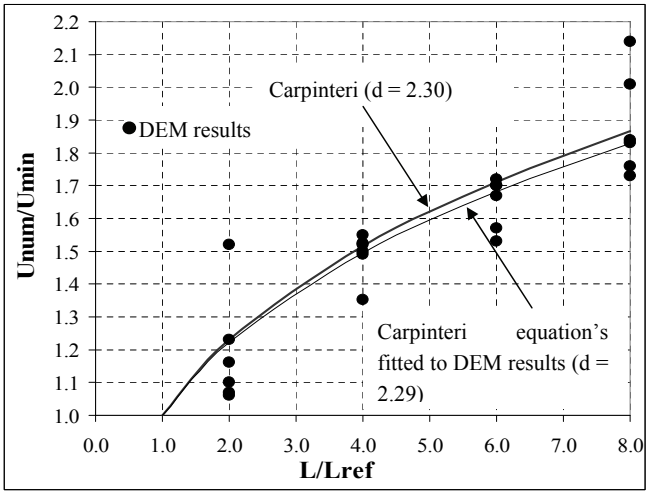

Figure 11: Comparison between Carpinteri and Chiaia (2002) and present DEM results, for uniform boundary displacements, showing the equation proposed by Carpinteri and Chiaia (2002) to simulated values obtained with DEM models (estimated fractal dimension d = 2.29).

large structures.

Acknowledgement: The authors acknowledge the support of CNPq and CAPES (Brazil).

References

Carpinteri, L., Chiaia, B. (2002): Embrittlement and decrease of apparent strength of large-sized concrete structures. *Sadhana*, Vol. 27, Part 4, 425-448, India.

Dalguer, L. A., Irikura, K., Riera, J. D., Chiu, H. C., (2001): The importance of the dynamic source effects on strong ground motion during the 1999 Chi-Chi, Taiwan, earthquake: brief interpretation of the damage distribution on buildings. *Bull. Seismol. Soc. Am.*, 91, 1112-1127.

Dalguer, L. A., Irikura, K., Riera, J. D. (2003): Simulation of tensile crack generation by three-dimensional dynamic shear rupture propagation during an earthquake. *J. Geophys. Res.*, 108(B3), 2144.

Hillerborg, A. (1971): A model for fracture analysis, Cod. LUTVDG/TVBM 300-51-8.

Iturrioz, I. (1995): Aplicação do método dos elementos discretos ao estudo de estruturas laminares de concreto armado. *Ph.D. thesis*, CPGEC, Universidade Federal do Rio Grande do Sul, Porto Alegre, Brazil.

Iturrioz, I., Miguel, L. F. F., Riera, J. D. (2009): Dynamic fracture analysis of concrete or rock plates by means of the Discrete Element Method. *Latin American Journal of Solids and Structures*, Vol. 6, pp. 229-245.

Leonhart, F., Walker, R. (1961): The Stuttgart shear tests, Translation No. 11, C&CA, London. *Beton und Stahlbetonbau*, Vol. 65, no. 12, 1961, Vol. 57, No. 2, 3, 7, 8.

Li, L., Liu, S., Wang, H. (2008): Meshless Analysis of Ductile Failure. *CMES: Computer Modeling in Engineering and Sciences*, Vol. 36, no 2, pp. 173-191.

Maiti, S., Geubelle, P. H. (2004): Mesoscale modeling of dynamic fracture of ceramic materials. *CMES: Computer Modeling in Engineering ans Sciences*, Vol.5, no. 2, pp.91-101.

Miguel, L. F. F. (2005): Critério constitutivo para o deslizamento com atrito ao longo da falha sísmica. *Ph.D. thesis*, 229 pp., PPGEC, Escola de Engenharia, Universidade Federal do Rio Grande do Sul, Porto Alegre, Brazil.

Miguel, L. F. F., Riera, J. D., Dalguer, L. A. (2006): Macro constitutive law for rupture dynamics derived from micro constitutive law measured in laboratory. *Geophys. Res. Lett.*, 33, L03302, doi: 10.1029/2005GL024912.

Miguel, L. F. F., Riera, J. D. (2007): A constitutive criterion for the fault: modified velocity-weakening law. *Bull. Seismol. Soc. Am.*, 97(3), 915-925, doi: 10.1785/0120060107.

Miguel, L. F. F., Riera, J. D., Iturrioz, I. (2008): Influence of size on the constitutive equations of concrete or rock dowels. *International Journal for Numerical and Analytical Methods in Geomechanics*, Vol. 32, No. 15, pp. 1857-188. doi: 10.1002/nag.699.

Nayfeh, A. H., Hefzy, M. S. (1978): Continuum modeling of three-dimensional truss-like space structures. *AIAA Journal*, 16(8), 779-787.

Needleman, A. (1997): Numerical modeling of crack growth under dynamic loading conditions. *Comp. Mech.*, Vol. 19, no 6, 463-469.

Ramallo, J. C., Kotsovos, M. D., Danesi, R. D. (1995): Unintended out-of-plane actions in size effects tests of structural concrete. *Proceedings, 13th International Conference on Structural Mechanics in Reactor Technology (SMiRT 13)*, Porto Alegre, Brazil, Vol. 3, 351-357.

Riera, J. D., Iturrioz, I. (1998): Discrete elements model for evaluating impact and impulsive response of reinforced concrete plates and shells subjected to impul-

sive loading. *Nuclear Engineering and Design*, 179, 135-144.

Riera, J. D., Iturrioz, I. (2007): Size effects in the analysis of concrete or rock structures. *19th International Conference on Structural Mechanics in Reactor Technology (SMiRT 19)*.

Riera, J. D., Miguel, L. F. F., Dalguer, L. A. (2005): On the constitutive criteria for the fault: Influence of size and tensile cracks generation during rupture. *18th International Conference on Structural Mechanics in Reactor Technology (SMiRT 18)*, Beijing, China.

Rios, R. D., Riera, J. D. (2004): Size effects in the analysis of reinforced concrete structures. *Engineering Structures*, Vol 26, Issue 8, 1115-1125.

Sageresan, N., Drathi, R. (2008): Crack Propagation in Concrete Using Meshless Method. *CMES: Computer Modeling in Engineering and Sciences*, Vol. 32, no 2, pp. 103-112.

Selvadurai, A. P. S. (2009): Fragmentation of Ice Sheets during Impact. *CMES: Computer Modeling in Engineering and Sciences*, Vol. 52, no 3, pp. 259-277.

Shen, L. (2009): A rate Dependent Damage/Decohesion Model for Simulating Glass Fragmentation under the Material Point Method. *CMES: Computer Modeling in Engineering and Sciences*, Vol. 49, no 1, pp. 23-45.

Van Mier, J. G. M. (2003): Fracture processes in concrete connecting various length scales, *Recent developments in he modeling of Recent developments in he modeling of rupture in solids*, Proceedings of the International Symposium, Foz do Iguazú, Brazil, Editors Benallal, A. and Proença, S.P.B., p. 31-36 (ISBN: 2-11-094072-7):

Van Vliet, M. R. A., Van Mier, J. G. M. (2000): Size effects of concrete and sandstone, *Heron*, Vol 45, No.2, 91-108.

Wang, H. X., Wang, S. X. (2008): Analysis of Dynamics Fracture with Cohesive Crack Segment Method. *CMES: Computer Modeling in Engineering and Sciences*, Vol. 35, no 3, pp. 253-274.